第 38 卷第 3 期
2019 年 6 月

红 外 与 毫 米 波 学 报
J. Infrared Millim. Waves

Vol. 38, No. 3
June, 2019

文章编号: 1001 - 9014(2019)03 - 0296 - 07

DOI: 10.11972/j.issn.1001 - 9014.2019.03.007

A D-band communication transmitter module with a novel self-aligned microstrip line-to-waveguide transition

YANG Song-Yuan[1], YU Wei-Hua[1*], AN Si-Ning[2], Ahmed Hassona[2], Herbert Zirath[2], LYU Xin[1], Zhongxia Simon He[2]

(1. School of Information and Electronics, Beijing Institute of Technology, 100081, China;
2. Dept. Microtechnology and Nanoscience, Chalmers University of Technology, 41296, Sweden)

Abstract: A D-band (110 ~ 170 GHz) transmitter module, based on a novel self-aligned microstrip-to-waveguide transition, was demonstrated. The simulated average insertion loss of the transition is about 0.6 dB and return loss is better than 10 dB during working band. A D-band transmitter module was developed using such transition with resistive mixer and multiplier chips. The transmitter module operates between 110 ~ 153 GHz and provides a peak saturated output power of −4.6 dBm at 150 GHz and with 13.5 GHz 3 dB bandwidth from 145.8 to 159.3 GHz. 3 Gb/s wireless communication with this module at 145 GHz was demonstrated with spectrum efficient 64-QAM modulation.

Key words: transmitter module, waveguide transition, low-cost packaging, D-band
PACS: 84.40.-x, 84.40.Az

一种基于新型自组装微带-波导过渡的 D 波段通信发射机模块

杨宋源[1], 于伟华[1*], 安思宁[2], *Ahmed Hassona*[2], *Herbert Zirath*[2], 吕 昕[1], 何仲夏[2]

(1. 北京理工大学 信息与电子学院,北京 100081;
2. 查尔姆斯理工大学 微技术和纳米科学系,瑞典 哥德堡 41296)

摘要: 展示了一种基于新型自组装微带-波导过渡的 D 波段(110 ~ 170 GHz)发射机模块. 过渡结构的仿真平均插入损耗为 0.6 dB,回波损耗于带内基本优于 10 dB. 基于该过渡结构以及阻性混频器和倍频器芯片,设计了一种 D 波段发射机模块. 该发射机模块工作于 110 ~ 153 GHz,峰值输出功率于 150 GHz 可达 −4.6 dBm,3 dB 带宽为 145.8 ~ 159.3 GHz. 使用该模块进行了 64-QAM 高阶无线通信测试,测试传输速率为 3 Gb/s,验证了模块封装方案的实用性.

关 键 词: 发射机模块; 波导过渡; 低成本封装; *D* 波段

中图分类号: 84.40.-x; 84.40.Az **文献标识码:** *A*

Introduction

Millimeter wave technology market is estimated to be worth 2.3 billion USD by 2023 including various segments such as mobile telecommunication, military, defense, aerospace and automotive. Most applications in telecommunication and automotive are cost sensitive; even aerospace industry starts to seek commercial off-the-shelf (COTS) components to become cost effective [1].

Traditional millimeter wave components and subsystems are expensive due to the fact of low-yield manual assembly and high tool precision requirement of different parts. Novel packaging solution, which can tolerate more tooling error and assembling displacement while maintain performance would, become a key enabler of millimeter wave technology commercialization. D-band (110 ~ 170 GHz) devices are researched extensively for its wide available bandwidth and low atmospheric attenuation. Different frequency channels within D-band are already allocated by standardization authorities (i.e., FCC, ITU, ETSI), for example, mobile communication (141.5 ~

Received date: 2018-12-19, **revised date:** 2019-03-02 **收稿日期:** 2018-12-19, **修回日期:** 2019-03-02
Foundation items: Supported by the National Natural Science Foundation of China (61771057); Stiftelsen för Strategisk Forskning of Sweden (SE13-0020)
Biography: YANG Song-Yuan (1990-), male, Yunnan, B. S. degree. Research area involves microwave theory and technology. E-mail: 20091401@bit.edu.cn
* **Corresponding author:** E-mail: ywhbit@bit.edu.cn

147.5 GHz), inter-satellite communication (167 ~ 174 GHz) and automotive radar applications (131 ~ 137 GHz). Several publications have exhibited high data rate communication using highly integrated D-band chip sets implemented in different semiconductor processes. A 165 GHz transceiver chipset in SiGe technology was demonstrated [2], Two D-band transmitters chips were also designed and measured with ASK modulation at 2.5 Gbps and 10 Gbps data rates [3,4]. Measured at 18 Gbps data rates with 64-QAM modulation, a D-band transmitter chipset in InP technology was presented [5].

Although mentioned transceivers performed well at D-band, they are all based on on-wafer measurements. However, packaging is a critical step for utilizing chip sets at D-band in practical systems. One of the key design features of packaging is the chip to rectangular waveguide transition. The chip-to-waveguide transitions were widely researched and several examples have been demonstrated at D-band frequency [6-12].

These transitions can be categorized into three types according to the differences in complexity of manufacture and assembly, as Fig. 1 shows.

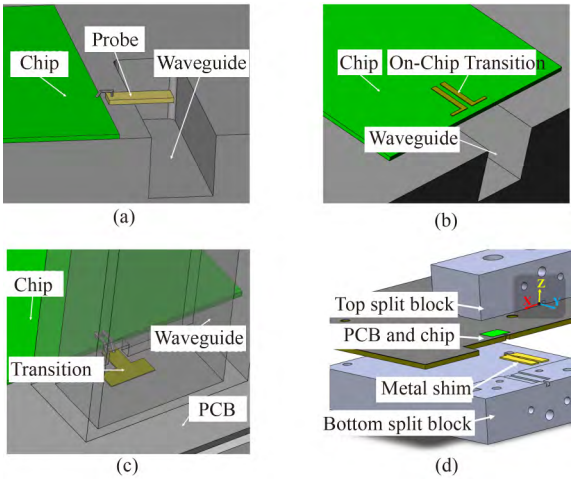

Fig. 1　3D diagrams of D-band transitions. (a) Probe type transitions, (b) On-chip Integrated transitions, (c) PCB transitions, (d) Conceptual exploding diagram of the proposed transition

图 1　D 波段过渡三维示意图. (a) 探针形式过渡, (b) 片上集成过渡, (c) PCB 过渡, (d) 本文提出过渡的爆炸视图

Probe type transitions [6-8] in Fig. 1(a) comprise of a low-loss E-plane probes, waveguide split blocks and a chipset which is wirebonded to the probe. The probes are independently fabricated by processes different from those of the chipsets. However, all three kind of parts need to be aligned carefully. The high requirement on the alignment precision limits the volume of production thus rise the cost of final product.

Some chipsets have integrated E-plane probe, as shown in Fig. 1(b) which avoid the alignment and wirebonds between chips and probes. Such chipsets can be aligned with high accuracy in the metal split blocks by using automatic pick-and-place machine [10-11]. To avoid high-order mode propagation, the probe size should not exceed certain critical size. This also limits the size of the chip or arises need of heterogeneous chip shape [11].

Both mentioned solutions directly attached the chipset onto waveguide metal blocks. Replacing damaged chipset in such modules would require extremely accurate operation in case of damaging the expensive waveguide metal blocks. To address this problem, PCB based packaging solutions have been proposed at V-band (52 ~ 67 GHz) [13] and at F-band (90 ~ 140 GHz) [14], as Fig. 1 (c) shows. By designing a PCB with E-plane probe separates the chipset-PCB assembly and PCB-waveguide assembly. Upon chipset damage, the module can be repaired easily by replacing the PCB.

At high frequency, the decreasing on width and spacing of PCB traces requires advanced manufacturing process with rigorous tolerance requirements (typical requirements are 80 μm line width, 80 μm spacing and 100 μm VIA diameter). The high cost and limited yield of advanced PCB process hinder the potential of successful commercialization.

In this paper, a transition solution comprising a low cost PCB, a thin-metal shim and metal split blocks is proposed, as Fig. 1(d) shows. The thin-metal shim can be manufactured easier with high precision. Therefore, a low cost PCB process with less precision requirement can be used without performance compromise at high frequency. Chip sets are mounted on the PCB, then the PCB is assembled between waveguide split blocks. Upon chipset damage, the module can be repaired by simply replacing a PCB.

Using a D-band transmitter module developed with the proposed transition, wireless data transmission experiments are performed and 64-QAM modulation at 3 Gbps data rate is demonstrated. Compared with published works [5,15-19] in the similar band, this work is one of them with relatively high spectral efficiency, as Fig. 2 shows.

This paper is organized as follows. Section 1 discusses the details of the transition design, choice of transmitter chip sets. In Section 2, the overview of measurement setups and measurement results are given.

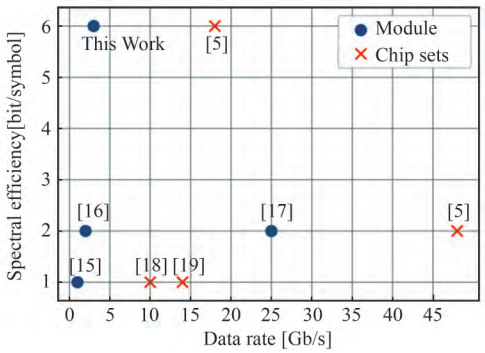

Fig. 2　Performance comparison on data rate and spectral efficiency

图 2　数据率和频谱效率的性能对比图

1　Transmitter Module Design

1.1　Transition Design

The proposed transition comprises a PCB, a metal shim and waveguide split blocks. The PCB has a 50 um ULTRALAM 3850 HT layer, a 50 um ULTRALAM 3908

bonding layer [20,21] and a 1 mm back copper. The equivalent microwave substrate is 100 μm with dielectric constant $\varepsilon_r = 3.5$ and loss tangent $\delta = 0.005$ at D-band [22]. The MMICs are mounted on the PCB and connected to a microstrip line (MSL) on the PCB by wirebonding. The MSL is extended to the edge of the PCB where the 1 mm copper back metal is removed at the edge, as Fig. 3 shows. Instead, shown in Fig. 4 a metal shim, whose shape partly matches to the PCB edge, is self-aligned to the back of the PCB. Part of the metal shim extends into the waveguide between spilt-blocks.

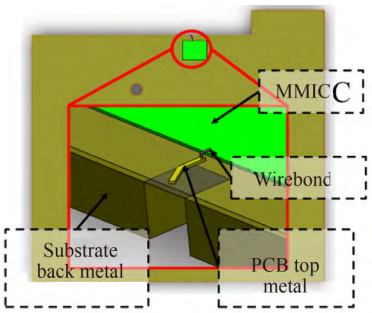

Fig. 3 The zoom-in diagram of PCB on which MMICs are mounted

图3 有MMIC装载的PCB过渡放大示意图

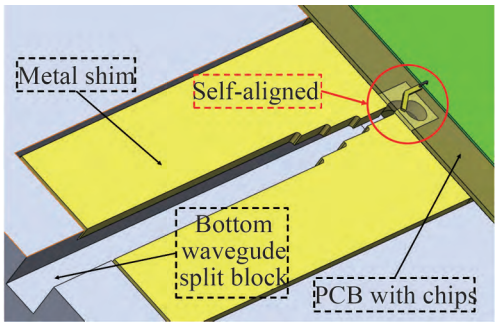

Fig. 4 The metal shim self-aligns with the PCB by the removed place of copper

图4 通过背面铜开槽和PCB对准的金属片

The RF signal from the MMIC starts as MSL mode. Through several intermediate modes transformation, a rectangular waveguide TE10 mode is established at the output. In Fig. 5, the propagation mode at different position of the transition is marked. Firstly, signal flows through a bond wire from a chip pad to a MSL on the PCB. At the end of the MSL (M-S plane), a slot opens on the metal shim (ground layer). This slot helps the field convert from MSL mode into slot line mode [23-25]. Notice that part of the shim is extended into the waveguide and forms a ridge waveguide configuration from S-R plane to R-W plane. A ridge waveguide binomial multisection matching transformer [26] is implemented on the shim. Then the ridge waveguide mode is converted into rectangular waveguide TE_{10} mode after R-W plane.

The simulated structure of the proposed transition in detail is shown in Fig. 6. As Fig. 6(a) shows, there is

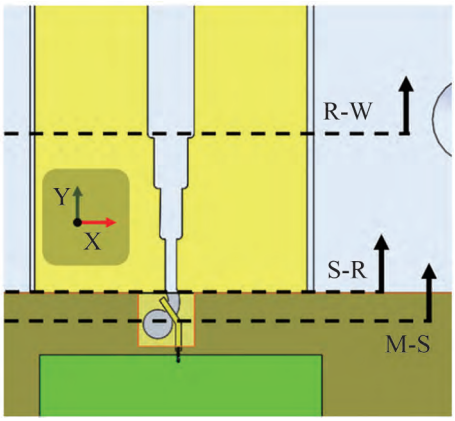

Fig. 5 Mode transformation of signal from MSL on chips to waveguide

图5 从芯片上的微带线(MSL)到波导的信号模式转换

a wide opening area on the top of the PCB. To avoid unwanted propagating mode, a bed of nails is implemented to form Perfect magnetic conductor (PMC) structure [27].

Ansoft HFSS software is used to simulate and optimize the transition. The critical dimensions of the transition after optimization are marked in Fig. 6(b) and summarized in Table 1.

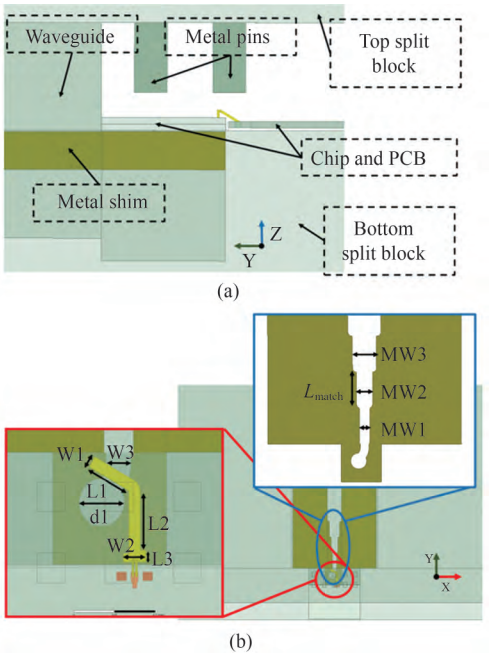

Fig. 6 Simulated model of MSL-waveguide transition. (a) YZ plane view, (b) XY plane view

图6 MSL-波导过渡的仿真模型. (a) YZ面视图, (b) XY面视图

The thickness of metal shim is chosen as 0.3 mm for easy fabrication. Several approaches can be used for shim fabrication including milling, chemical etching and laser cut with typical tolerance less than 10 μm. In this work, milling is used for shim fabrication with less than 2 um accuracy. Under such high accuracy, the fabrication

Table 1　Critical dimensions of the proposed transition
表 1　过渡结构的关键几何尺寸

Parameter	Dimension/mm	Parameter	Dimension/mm
W1	0.1	MW1	0.26
L3	0.1	M21	0.4
L1	0.405	MW3	0.6
L2	0.5	L_{match}	0.9
W2	0.2		
W3	0.22		
d1	0.6		

error influencing transition S-parameters can be ignored.

The simulated S-parameters of the proposed transition is shown in Fig. 7. The average insertion loss of this transition is about 0.6 dB and return loss is better than 10 dB covering frequencies from 110 GHz to 153 GHz. Even though the metal shim is self-aligned during assembling, assembling error can still appear. Such assembly offset error is also simulated as part of tolerance study. The maximum shifting along the x-y plane of 100 um results in about only 3 GHz bandwidth reduction from upper bound, also shown in Fig. 7.

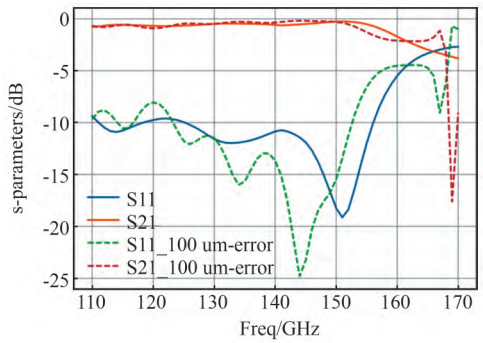

Fig. 7　Simulated S-parameters and assembling error of the proposed transition
图 7　过渡结构仿真 S 参数及装配误差

In TABLE II, a comparison is made with state-of-the-art D-band transitions. The proposed transition exhibits wide bandwidth, qualified performance and relatively low cost. Although the transition in Ref. [12] has better performance and the similar manufacture process, the proposed transition is more compact. The length of the transition [12] is 2.68 mm, which is much longer than 0.945 mm in the proposed transition.

1.2　Transmitter Assembling Details

To demonstrate the proposed transition, a transmitter module is built using a heterodyne architecture as shown in Fig. 8. Differential quadrature (IQ) intermediate frequency (IF) signals were input into a D-band balanced sub-harmonic resistive mixer (Gotmic gMDR0035 A). According to its datasheet [28], this mixer can work with IF input signals from DC to 6 GHz and RF output signals from 140 to 170 GHz. The mixer chip can achieve a maximum saturated power of -2 dBm and typical conversion loss (CL) of 12 dB. The mixer is driven by a 15 dBm Local oscillator (LO) signal at frequencies from 70 to 85 GHz. A frequency sextupler chip (Gotmic gXSB0025 A) is used as a LO source which requires 5 dBm input at frequencies from 11.8 ~ 14.4 GHz [29].

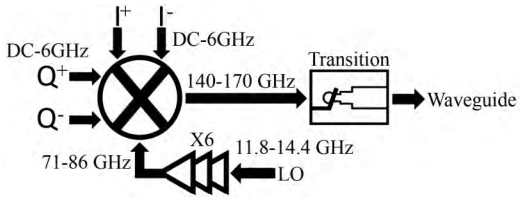

Fig. 8　Block diagram of D-band transmitter. The transition transforms electromagnetic wave from MSL mode into rectangular waveguide mode
图 8　D 波段发射机框图. 过渡结构把电磁波从 MSL 模式转换到方波导模式

A resistive mixer is preferred due to its excellent linearity. Though the mixer has 12 dB conversion loss, it is still able to provide a sufficient output power for wireless communication demonstration.

The photographs of the transmitter module, including the mounting of chipsets, the proposed transition, the top split block and the assembled transmitter module are shown in Fig. 9, Fig. 10 and Fig. 11 respectively.

2　Measurements Results

2.1　Spectral Domain Measurements

To measure the transmitter module, mixer measurement mode of Keysight PNA-X and a D-band VDI frequency extender were used. As Fig. 12 shows, the quad-

Table 2　Measurements comparison of D-band transition
表 2　D 波段过渡测试对比

No.	Process	Measured Topology	Bandwidth	Freq band/GHz	Insertion Loss/dB[a]	Return Loss/dB[b]
[7]	4 μm-thick HMDS-N	–	16.39%	140 -165	2.5	20
[8]	50 μm-thick quartz	Back-to-Back	14.29%	130 -150	0.55	15
[9]	eWLB	Single-side	26.22%	116 -151	3.4	5
[10]	CMOS	Transition + Antenna	15%	120 -160	–	6
[12]	Rogers 5880	Back-to-Back	30.77%	110-150	0.54	10
This work	Rogers 3850	Single-side[c]	31.42%	110-165	0.6	5
		Active circuits + Transition	8.8%	145.8-159.3[d]	–	–

[a] Average insertion loss.
[b] Maximum return loss.
[c] Simulated results.
[d] 3 dB output power bandwidth.

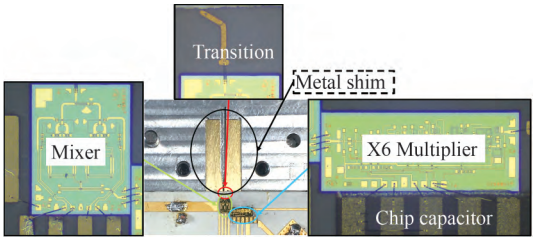

Fig. 9 Photographs of chip sets mounted on the bottom split block; chip capacitors were used for DC power decoupling

图9 装配在下腔体上的芯片组照片;芯片电容用来解耦支流供电

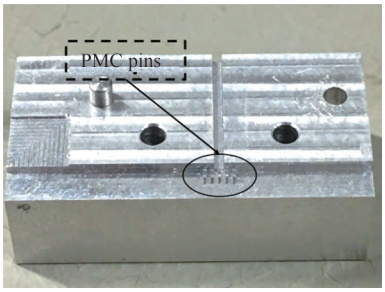

Fig. 10 Top split block with PMC pins

图10 有PMC柱的上腔体

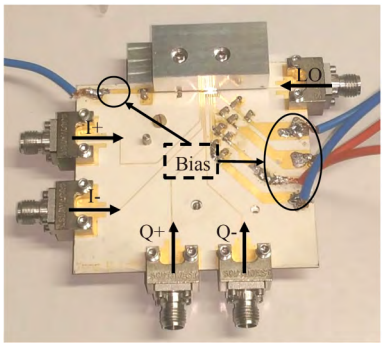

Fig. 11 Assembled transmitter module

图11 装配好的发射机模块

rature differential input signal was generated by PNA-X through a quadrature coupler and two baluns. The LO signal with relative high power was also generated by PNA-X. The D-band output port was directly connected with waveguide port of the VDI extender.

After implementing the standard calibration steps of mixer measurement mode, the CL and output power can be measured. To compare with measurement results in chip datasheets, we adjusted the bias condition into best working status and 5 dBm LO power is provided to the module, as recommended by the datasheets.

Fig. 13 shows the measured CL versus input power. The measurement results are plotted with on-wafer measurement result (extracted from data sheet). It can be seen that the measured results fit well with on-wafer

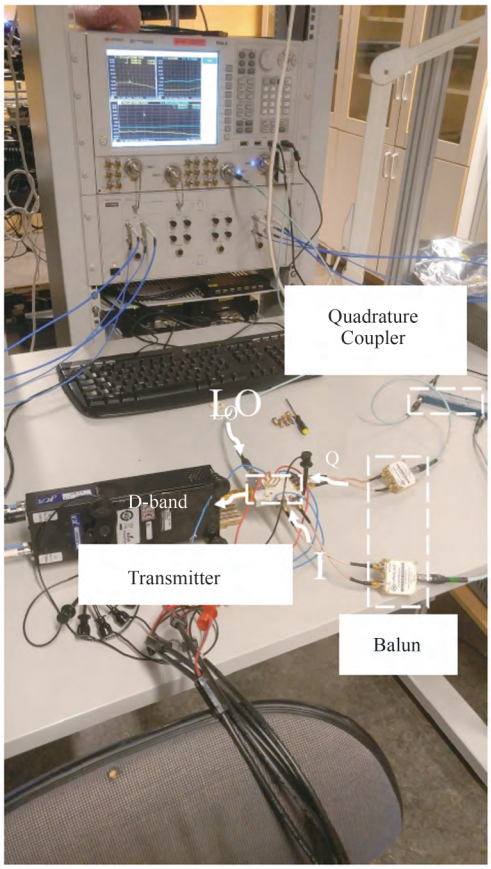

Fig. 12 Photograph of CL and saturated power measurement setup for the transmitter module

图12 发射机的变频损耗和饱和功率测试平台照片

measurement when input power is lower than 5 dBm. At higher input power levels, the measured CL gradually higher than results from the datasheet. Nevertheless, the transmitter module shows an output 1 dB compression point of 4 dBm.

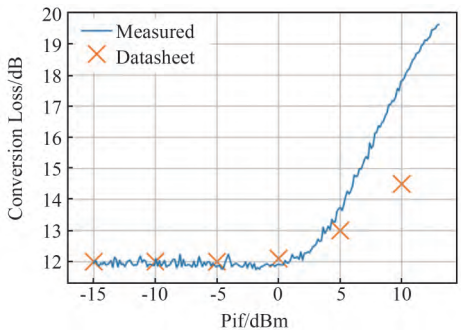

Fig. 13 Conversion loss (CL) at output frequency of 145 GHz vs. IF input power at 1 GHz

图13 射频输出145GHz时的变频损耗vs. 1GHz的中频输入功率

Fig. 14 shows the measured CL versus IF frequency with a fixed LO signal at 155 GHz, also in comparison to the on-wafer measured results. The measured results can fit with results from the datasheet well except for small

deviation at high IF frequency. It can be seen 3 dB bandwidth of 6 GHz is obtained with the transmitter module as expected.

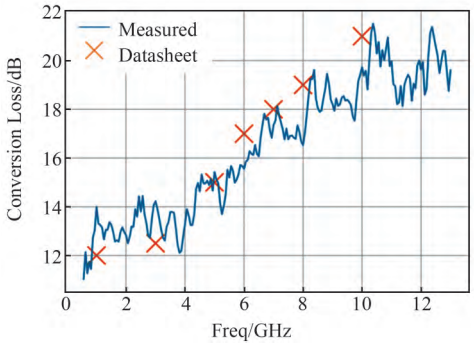

Fig. 14　Conversion loss (CL) at RF of 145 GHz vs. IF input power at 1 GHz
图 14　射频输出 145 GHz 时,变频损耗 vs. 1 GHz 的中频输入功率

Fig. 15 shows the measured CL versus different LO input frequencies with a fixed 1 GHz IF signal input (P_{if} = −20 dBm). The measured results agree well with on-wafer test from the datasheet at output frequencies lower than 155 GHz. Higher than 155 GHz, the transmitter module shows higher CL potentially due to insufficient LO power to the mixer as well as higher loss of the PCB transition.

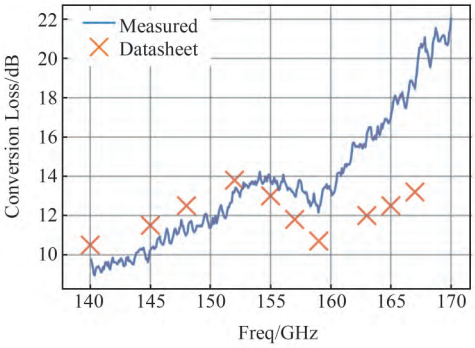

Fig. 15　Conversion loss (CL) vs. output frequency with IF signal at 1 GHz
图 15　中频信号为 1GHz 时,变频损耗 vs. 输出频率

Fig. 16 shows the saturated output power versus output frequency with IF frequency at 1 GHz. The peak saturated output power (P_{sat}) is −4.6 dBm at 150 GHz. The P_{sat} is 2.6 dB lower than that of mixer chip from datasheet, −2 dBm.

The 3 dB bandwidth of the saturated output power is 13.5 GHz, which is from 145.8 to 159.3 GHz. At frequency higher than 159.3 GHz, the power decreases rapidly for the transition's performance decreases.

2.2　Time Domain Measurements

The proposed transmitter module is used in a wireless communication demonstration. An InP DHBT based receiver module [30] is used as a corresponding receiver. A Keysight M8195A arbitrary waveform generator (AWG) is used to generate modulated differential quad-

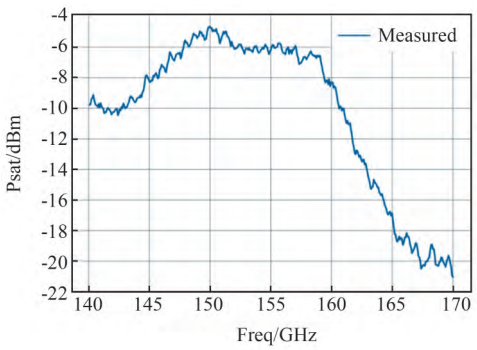

Fig. 16　Saturated output power vs. output frequency with IF signal at 1 GHz
图 16　中频信号为 1 GHz 时,饱和输出功率 vs. 输出频率

rature IF signals at 1 GHz (I+, I−, Q+ and Q−) for the transmitter. A 20 dBi waveguide interfaced corrugated horn antenna is used at transmitter side. The receiver module locates at 50 cm away using a 21 dBi horn antenna. The transmitter and receiver modules use different LO source, the received I and Q signals are connected to a Teledyne LECROY LabMaster 10 Zi-A Oscilloscope. Lecroy Vector-Signal-Analyzer (VSA) software package is used to perform carrier recovery and demodulation. The photo of the laboratory setup is shown in Fig. 17.

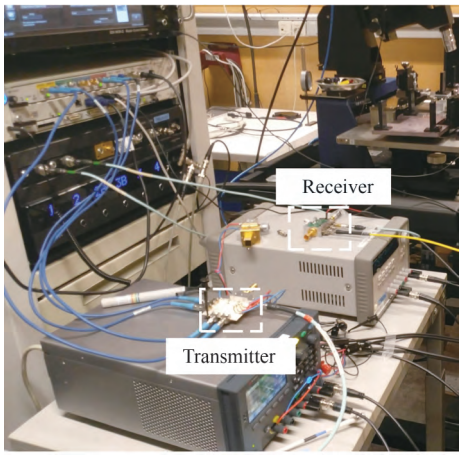

Fig. 17　Photograph of the constellation measurements setup
图 17　星座图测试平台照片

A 3-Gbps 64-QAM signal is transmitted over 0.5 m wireless link and the received constellation is shown in Fig. 18. The measured error-vector magnitude (EVM) is 4.86%.

3　Conclusion

A D-band transmitter module, based on commercial resistive mixer and multiplier chip sets, with low-cost and compact transition was demonstrated. This transmitter module supports 3-Gbps data rate 64-QAM modulated wireless communication. All parts of the module are made by commercial available manufacture and assembly

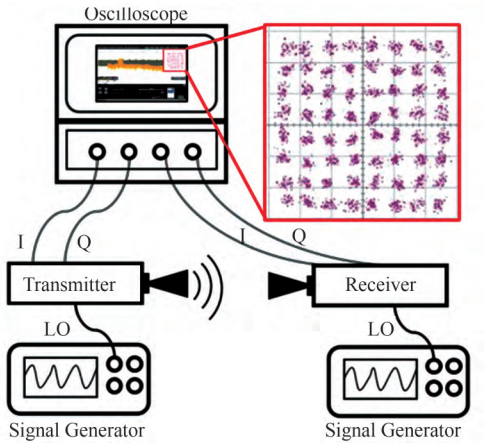

Fig. 18 The block diagram of 64-QAM measurement set-up and measured constellation

图 18 64-QAM 测试平台框图及测试的星座图结果

process.

References

[1] Millimeter Wave Technology Market by Product (Scanner Systems Telecommunication Equipment) , Frequency Band, License Type, Application (Mobile and Telecom, Military, De-fense, and Aerospace, Automotive) , and Geography-Global Forecast to 2023 [OL] , 2017, https: //www. marketsandmarkets. com/Market-Reports/millimeter-wave-technology-market-981. html.

[2] Laskin E. Chevalier, P. Chantre , A. , *et al*. 165 GHz Transceiver in SiGe Technology [J] . *IEEE Journal of Solid-State Circuits*, 2008, **43** (5) : 1087-1100 [3] Xu Z. Gu, Q. J. ,Wu Y. -C. , *et al*. Chang, D-band CMOS transmitter and receiver for multi Giga-bit/sec wireless data link: IEEE Custom Integrated Circuits Conference [C] . USA : 2010: 1-4.

[4] Katayama K, Motoyoshi, M Takano K, *et al*. 28mW 10Gbps transmitter for 120 GHz ASK transceiver: IEEE/MTT-S International Microwave Symposium Digest [C] . Canada: 2012: 1-3.

[5] Carpenter S. Nopchinda, D. ,Abbasi M. , *et al*. A D-band 48-Gbit/s 64-QAM/QPSK Direct-Conversion I/Q Transceiver Chipset [J] . *IEEE Transactions on Microwave Theory and Techniques*, 2016, **64** (4) : 1285-1296.

[6] Mullerwiebus V. Experimental characterization and behavior to misalignments of a D-band-transition from rectangular to coplanar waveguide on membrane: Conference Digest of the Joint International Conference on Infrared and Millimeter Waves and International Conference on Terahertz Electronics [C] . Germany: 2004: 481-482.

[7] Hirsch S, Duwe K, Judaschke R. A transition from rectangular waveguide to coplanar waveguide on membrane: 25th International Conference on Infrared and Millimeter Waves (Cat. No. 00EX442) [C] . China: 2000: 299-300.

[8] Roy R, Kush A K, Dixit R P. Fabrication and performance of broadband back to back waveguide to suspended stripline transition on quartz for D-band: International Conference on Recent Advances in Microwave Theory and Applications [C] . India: 2008: 719-721.

[9] Hassona V, Vassilev Z. S. He, *et al*. Silicon Taper Based D-band Chip to Waveguide Interconnect for Millimeter-Wave Systems [J] . *IEEE Microwave and Wireless Components Letters*, 2017, **27** (12) : 1092-1094.

[10] Deng X D, Li Y, Wu W, *et al*. A D-band chip-to-waveguide-horn (CWH) antenna with 18. 9 dBi gain using CMOS technology: Wireless Symposium [C] . China: 2015: 1-4.

[11] Hassona, Z. S. He, V. Vassilev, *et al*. D-band waveguide transition based on Linearly Tapered Slot Antenna: IMAPS Nordic Conference on Microelectronics Packaging (NordPac) [C] . Sweden: 2017: 64-67.

[12] Wang J. , Hao Z. C. , Fan K. K. . A 110-150 GHz SIW-rectangular waveguide transition for terahertz applications: IEEE Mtt-S International Microwave Workshop Series on Advanced Materials and Processes for RF and THz Applications [C] . China: 2016: 13.

[13] M. Fakharzadeh and S. Jafarlou. A Broadband Low-Loss 60 GHz Die to Rectangular Waveguide Transition [J] . *IEEE Microwave and Wireless Components Letters*, 2015, **25**(6) : 370-372.

[14] Jameson S. ,Khamaisi B. Socher E. . A +6 dBm 128GHz source module with full F-band waveguide package and wirebonded CMOS chip: IEEE MTT-S International Microwave Symposium (IMS) [C] . USA: 2016: 1-4.

[15] Li, S. Chi T. Park, J. S. , *et al*. A fully packaged D-band MIMO transmitter using high-density flip-chip interconnects on LCP substrate: IEEE MTT-S International Microwave Symposium (IMS) [C] , USA: 2016: 1-4.

[16] Deferm N. Reynaert P. . A 120 GHz Fully Integrated 10 Gb/s Short-Range Star-QAM Wireless Transmitter With On-Chip Bondwire Antenna in 45 nm Low Power CMOS [J] . *IEEE Journal of Solid-State Circuits*, 2014, **49**(7) : 1606-1616.

[17] Takahashi H. ,Hirata A. ,Takeuchi J. , *et al*. 120-GHz-band 20-Gbit/s transmitter and receiver MMICs using quadrature phase shift keying: 7th European Microwave Integrated Circuit Conference [C] . Netherlands: 2012: 313-316.

[18] Kosugi T. Tokumitsu, M. ,Enoki T. , *et al*. 120-GHz Tx/Rx chipset for 10-Gbit/s wireless applicationsusing 0. 1 mu; m-gate InP HEMTs: IEEE Compound Semiconductor Integrated Circuit Symposium [C] . USA: 2004: 171-174.

[19] Foulon S. ,Pruvost S. ,Pache D. , *et al*. A 142 GHz fully integrated wireless chip to chip communication system for highdata rate operation: Proceedings of the ESSCIRC (ESSCIRC) [C] . Romania: 2013: 77-80.

[20] R. Corporation. ULTRALAM 3850, Liquid Crystalline Polymer, laminate circuit materials [OL] , 2015, https: //www. rogerscorp. com/documents/730/acm/ULTRALAM-3000-LCP-laminate- data-sheet-ULTRALAM-3850. aspx.

[21] __, ULTRALAM 3908 Bondply [OL] , 2015, http: //www. rogerscorp. com/documents/731/acm/ULTRALAM-3000-LCP-PrepregULTRALAM-3908.

[22] Smith S. L. Dyadyuk V. . Measurement of the dielectric properties of Rogers R/flex 3850 liquid crystalline polymer substrate in V and W-band: Antennas and Propagation Society International Symposium [C] , USA: 2005: 435-438.

[23] Behera B. R. . Vivaldi antenna for medical applications: Design, modelling and analysis of microstrip-fed vivaldi antenna: IEEE Annual India Conference (INDICON) [C] . India : 2016: 1-4.

[24] Ren X. ,Liao S. Xue, Q. , *et al*. Wideband circularly polarized antenna based on Vivaldi antenna structure: IEEE International Symposium on Antennas and Propagation USNC/URSI National Radio Science Meeting [C] . USA: 2017: 1321-1322.

[25] Dong Y. ,Choi J. Itoh, T. . Vivaldi Antenna With Pattern Diversity for 0. 7 to 2. 7 GHz Cellular Band Applications [J] , IEEE Antennas and Wireless Propagation Letters,2018, **17**(2) : 247-250.

[26] Pozar D. M. . Microwave Engineering [M] . USA: John Wiley & Sons, Inc, 2011, 252-256.

[27] Kildal P. S. Alfonso, E. , A. Valero-Nogueira, *et al*. Local Metamaterial-Based Waveguides in Gaps Between Parallel Metal Plates [J] , *IEEE Antennas and Wireless Propagation Letters*, 2009, **8**: 84-87.

[28] Gotmic, Datesheet of D-band IQ-subharmonic mixer MMIC (gMDR0035 A) [OL] , http: //www. gotmic. se/documents/gMDR0035A.

[29] Gotmic, Datasheet of E-band X6 MMIC multiplier (gXSB0025 A) [OL] , 2016, http: //www. gotmic. se/documents/gXSB0025A.

[30] Vassilev V. He,, Z. S. S. Carpenter, *et al*. Spectrum Efficient D-band Communication Link for Real-time Multi-Gigabit Wireless Transmission: IEEE MTT-S International Microwave Symposium (IMS) [C] , USA: 2018: 1523-1526.